IEEE Access
Multidisciplinary | Rapid Review | Open Access Journal

Received 3 May 2024, accepted 17 May 2024, date of publication 24 May 2024, date of current version 4 June 2024.

Digital Object Identifier 10.1109/ACCESS.2024.3405393

RESEARCH ARTICLE

Experimental Evaluation and Modeling of the Accuracy of Real-Time Locating Systems for Industrial Use

SEPIDEH VALIOLLAHI[1], IGNACIO RODRIGUEZ[2], WEIFAN ZHANG[1], HIMANSHU SHARMA[1], AND PREBEN MOGENSEN[1]

[1]Wireless Communication Networks Section, Department of Electronic Systems, Aalborg University, 9220 Aalborg Øst, Denmark
[2]Area of Signal Theory and Communications, Department of Electrical Engineering, University of Oviedo, 33203 Gijón, Spain

Corresponding author: Sepideh Valiollahi (svbi@es.aau.dk)

This work was supported in part by the Innovation Fund Denmark through the Project "5G-ROBOT—5G Enabled Autonomous Mobile Robotic Systems," in part by Spanish Ministry of Science and Innovation under Ramon y Cajal Fellowship funded by MCIN/AEI/10.13039/501100011033; and in part by the European Social Fund "Investing in Your Future" under Grant RYC-2020-030676-I.

ABSTRACT Real-time locating systems (RTLSs) have proven to be a practical and effective solution for monitoring positions/status of humans and other entities in industrial environments, ensuring safe and efficient automated operations, by responding in real-time to unexpected events, such as the proximity of human workers to autonomous mobile robots (AMRs). This work focuses on evaluating and modeling the performance of two complementary RTLSs targeting human localization in both static and mobile conditions within a realistic industrial environment in operational conditions; with the aim of integrating live positioning information into digital twins (DT) for industrial use. Both the primary RTLS examined, an ultra-wide band (UWB) radio-based system; and the secondary RTLS, an optimized camera vision (CV)-based system with three surveillance cameras introduced as a backup RTLS, exhibited a similar median accuracy of 12-13 cm in static conditions, being the one of the UWB system slightly degraded down to 19 cm in presence of human shadowing. In human mobility conditions, the median accuracy values were further debased by 4 and 13 cm for the UWB and CV systems, respectively, indicating a limited real-time fluctuation, sufficiently bounded to guarantee the safety of human workers based on the readings of either of the primary or secondary RTLS systems. Based on the observed performance, a safety protocol for human detection in operational production scenarios was established, considering operational safety margins around humans of 1-2 m, which could be further leveraged by centralized monitoring and control entities such as industrial digital twins. The localization accuracy of the systems is characterized by means of error functions quantifying the distance to ground truth (GT) points through Gamma distribution functions using maximum likelihood estimates (MLEs). The proposed models are practical for implementation in system level simulators or industrial digital twin tools considering akin industrial environments. The different observations presented along the paper are useful for advanced industrial operation planning and optimization considerations.

INDEX TERMS Smart factories, real-time locating systems, ultra-wideband, camera-vision, human workers, autonomous mobile robots, digital twins, localization error models.

I. INTRODUCTION

In line with the increasing emphasis on Industry 4.0 and the drive towards maximizing autonomous production processes, the importance of ensuring both efficiency and safety within manufacturing operations becomes apparent. This becomes particularly crucial in situations where human workers coexist with autonomous mobile robots (AMRs), and when unexpected events arise within the production area. To ensure seamless workflows, it is necessary for both human and robotic entities to have awareness of each other's positions. This forms the core motivation behind the adoption of indoor

The associate editor coordinating the review of this manuscript and approving it for publication was Riccardo Carotenuto.

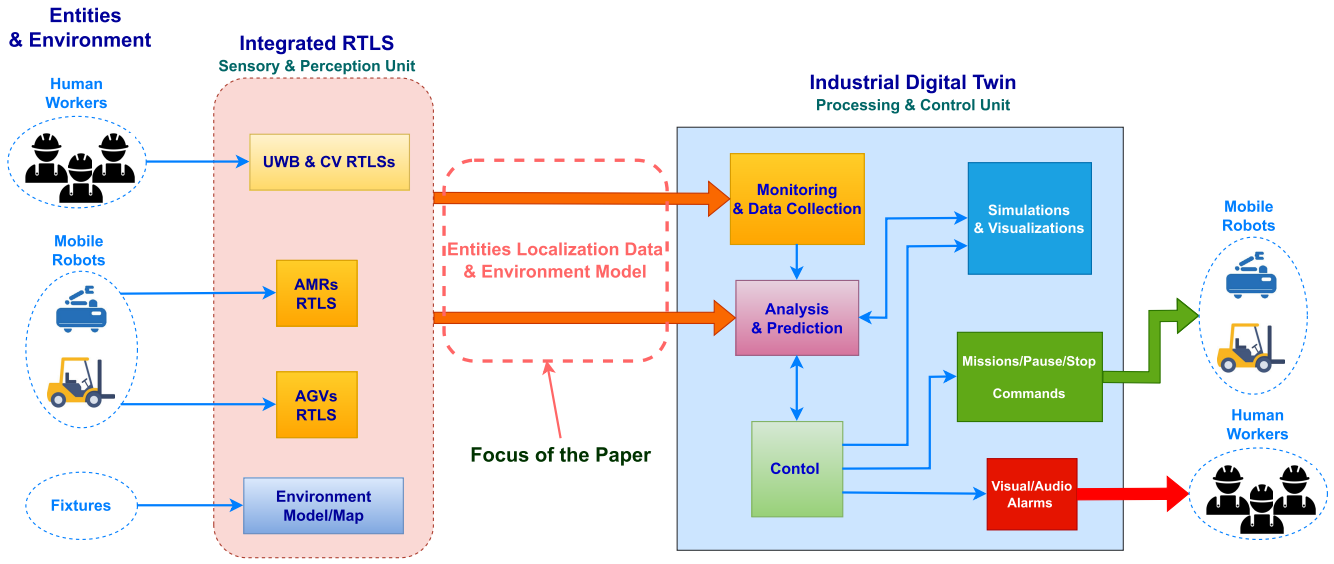

FIGURE 1. Real-time locating systems in closed control loop with industrial digital twin for real-time production planning, validation, and modification.

real-time locating systems (RTLSs) in smart factories. Indoor industrial environments typically are global positioning systems (GPS)-denied environments and, therefore, indoor RTLSs are used instead to continuously monitor the production area and provide real-time localization data, tracking locations of human workers and objects [1], as robotic entities such as AMRs already possess precise built-in localization and navigation mechanisms typically based on light detection and ranging (LiDaR) and inertial measurement unit (IMU) sensors technology [2]. Although AMRs are equipped with on-board sensors to construct internal maps of their surroundings, they often struggle to detect humans and other non-stationary objects in advance due to non-line-of-sight (NLOS) situations. Consequently, this can result in unnecessary delays, interruptions, or the risk of getting stuck in deadlocks. By leveraging real-time localization data, RTLSs empower AMRs to accurately perceive their surroundings in a timely manner to adapt their paths accordingly, ensuring smooth and efficient navigation [3], [4].

The increasing complexity of industrial systems and production processes in smart factories is pushing towards operational optimization strategies based on the centralization and integration of available information [5]. This information is gathered from the multiple control and monitoring systems available at all levels of the manufacturing process as defined by the automation pyramid [6]: from top management and planning levels, at which enterprise resource planning (ERP), manufacturing execution system (MES), or warehouse management system (WMS) information is available; to bottom control and field level, at which operational control data from shop floor machinery is directly collected from controllers, sensors, and actuators. In general, until now, the higher management layers considered only summaries of the specific information from lower layers for monitoring purposes or to make high level control decisions. However, the introduction of digital twin (DT) technologies [7], [8], [9], [10] is changing this paradigm, as there is an aim of providing a virtual replica of the physical environment, enabling real-time monitoring, analysis, and optimization of production processes, which requires information and data from all layers.

Here, the inherent capability of the RTLSs to deliver continuous and precise localization data, becomes the fundamental driver behind the ability of optimizing industrial production processes, and swiftly responding to changing circumstances. Therefore, in this paper, we set out the focus on our vision, described in Fig. 1, of integrating multiple RTLSs as inputs within closed control loops, having an industrial DT as the processing core. Within this DT context, our primary goal revolves around integrating positioning information (live data and models) into digital twins for industrial use. To do this, we analyze, characterize, and model the outputs of the selected indoor RTLS targeting human worker localization and tracking in a reference industrial scenario under realistic operational conditions. In this case, a primary one based on ultra-wideband (UWB) radio and a secondary one based on camera vision (CV) serve as inputs to the DT for performing the advanced control computations for run-time optimization, as well as for carrying out emulated/simulated operational performance predictions based on realistic values and models [11], [12]. As depicted in Fig.1, this corresponds to the evaluation of the potential inputs to the "monitoring and data collection" and the "analysis and prediction" DT modules, which will enable the possibility of doing "simulations and visualizations" based on realistic human and AMR system dynamics. The combination of the available online and offline information at these modules will allow the DT to "control" (adjust

dynamically and optimize) the overall production operations by ''tuning missions or issuing commands'' to the robotic elements and/or ''issuing visual/audio alarms'' to humans in advance case of potential dangerous situations.

At this point, the crucial role of RTLS data as a primary source of information for an industrial DT for analysis and control decision-making should be clear. Consequently, a verified RTLS with a known or predictable accuracy, achieved through an estimated model, is a prerequisite for a reliable DT capable of planning efficient and safe production procedures. Therefore, the main contributions of the paper are summarized as follows:

- Performance evaluation and mathematical modeling of the accuracy of two human-centric RTLSs (UWB and CV) in an operational industrial environment, considering both static and mobile conditions.
- Quantitative assessment of the impact of the human body on UWB RTLS performance, utilizing wearable UWB tags.
- Optimization and integration of CV localization data from multiple surveillance cameras for enhanced accurate location estimation within key production areas.
- Establishment of environment-specific safety measures for detecting humans without UWB tags based on the concurrent performance evaluation of the two RTLSs.

These contributions are key to the further development of our integrated DT vision, as the different experimental results serve as technical performance reference for the selected human worker tracking RTLS. Further, the extrapolated mathematical models of the accuracy of the RTLS in the different conditions can be used in simulations considering similar industrial deployent conditions, abstracting the parametrization and complexity of real-time localization.

The rest of the paper is organized as follows. Section II addresses the specific selection of UWB and CV indoor RTLSs in the context of operational industrial scenarios, along with a review of the state-of-the-art focused mainly on operational accuracy and characterization/modeling of positioning errors. Section III describes the realistic operational industrial environment used in the experimentation and characterization, highlighting the main deployment aspects of the different RTLSs. Section IV presents the RTLSs performance evaluation, along with the accuracy modelling aspects and the discussion of the results, for different operational configurations. Finally, Section V provides the conclusion and a future outlook discussion.

II. RELATED WORKS

Among the numerous indoor RTLS technologies that rely on radio frequency (RF) signal exchange, such as Wi-Fi, Bluetooth, Infrared, and RFID; UWB stands out due to its exceptional combination of accuracy, reliability, scalability, real-time tracking capabilities, and low power consumption [13], [14]. These attributes have made of UWB a preferred choice for an efficient location tracking solution in industrial settings, achieving an operational accuracy in the range of 20 cm to over 100 cm, depending on the factory conditions [15].

While UWB transmitters are often utilized as wearable devices by human workers on factory floors [16], [17], it is noteworthy that no previous studies conducted in industrial environments have explored the impact of the human body on UWB RTLS performance. So far, research endeavors that have provided models for UWB inaccuracies in industrial settings have primarily focused on the effects caused by fixtures, such as multipath effects stemming from metal structures or the shadowing or NLOS effects induced by walls [18]. To the best of our knowledge, the studies addressing the influence of the human body on UWB performance have been conducted mainly in non-industrial environments [19], [20], [21], [22] and, therefore, further evaluation in industrial scenarios is needed to validate whether non-industrial results and models still apply in environments with such distinct layouts, system topologies, and overall radio propagation conditions [19]. In general, the effect of the human body on UWB accuracy reported in the literature for non-industrial environments is found to be dependent on the relative heading angle (RHA) between the UWB transmitter and receiver devices, leading to UWB ranging errors of up to 160 cm [20], with the forehead and the chest being the most and the least favorable device positions on the body, respectively [19]. In terms of ranging error modelling the literature considers, typically, a combination of low-sigma Gaussian and Gamma distributions, representing the line-of-sight (LOS) and NLOS situations, respectively [19], [20], [23], [24].

Despite the peerless features of UWB RTLS, one potential drawback is the reliance on individuals wearing UWB tags for accurate localization. If individuals forget to wear their tags or if the tags run out of battery, their location cannot be tracked using the UWB RTLS system, which is often ignored in related studies [25]. This limitation can introduce challenges in maintaining consistent tracking coverage and thus require backup RTLS systems, to mitigate the impact of missing or inactive tags. In this context, CV-based RTLSs offer distinct advantages over other tracking technologies used as the backup system [26], [27], [28]. These include: no reliance on additional equipment, precise identification and tracking through advanced algorithms, comprehensive coverage using multiple cameras, additional insights through behavior analysis and anomaly detection, and seamless integration with existing infrastructure [29], [30], [31].

The accuracy of CV-based RTLSs highly depends on the camera type/position, coverage area, calibration method, detection algorithm, and type of detected elements (i.e. artificial markers or real features); as it can vary from meter ranges even to millimeter ranges in strictly controlled environments [32]. Generally, studies that are somewhat analogous to our research, involving the utilization of static surveillance cameras in indoor settings for human detection based on physical characteristics, have reported distances ranging from 15 cm to 60 cm [30], [33], [34], [35], [36]. A majority of studies addressing the sources/models of

localization error in CV systems have focused on stereo systems [37], [38], as contrary to monocular CV systems. The authors in [39] utilized an object detection algorithm with a thermal imaging dataset of an infrared camera to assess pixel-wise localization errors for detected objects. They modeled these errors as normal distributions, varying with the distance of the objects from the camera. This information was then used to create a spatial error distribution, projected onto the world coordinate system using the camera transformation matrix. This process resulted in an elliptical error distribution around the object, with a more significant error in the y-pixel direction than the x-pixel direction, highlighting that the uncertainty of localization measurement depends on both the sensor and the processing algorithm.

Specifically in human surveillance applications covering extensive areas, such as factory floors, the utilization of multiple cameras is crucial to ensure comprehensive coverage [40]. However, this introduces the challenge of either consolidating their individual outputs or establishing a cohesive network among them [41]. Various approaches are employed to tackle this challenge. Some methods, known as pre-processing approaches, integrate cameras during frame processing, utilizing all captured frames from each camera while applying detection/tracking algorithms [42], [43]. Although these approaches may result in more accurate human localization, achieving precision up to 5 cm, they demand significant processing power proportional to the number of cameras and often require overlapping fields of view. Conversely, post-processing approaches, which involve the fusion of detection/tracking outputs from individual cameras [44], [45], offer greater flexibility. These methods are more adaptable to different setups and better suited for real-time applications, though they typically achieve slightly lower accuracy, around 20 cm. Additionally, post-processing camera fusion algorithms that operate independently of specific camera setup knowledge, such as model or position, exhibit superior generalization capabilities. This independence allows them to incorporate more cameras effectively or be applied to varied setups, enhancing their utility across diverse surveillance scenarios. A concise summary of the literature discussed is presented in Table 1.

III. MEASUREMENT SETUP AND METHODOLOGY

As mentioned earlier in Section I, to guarantee a high level of safety and efficiency for both humans and mobile robots, complementary RTLSs are needed in order to backup each other in case of one's failure in sending real-time localization/positioning data. Stemming from our motivation to leverage this paradigm, we evaluate and model localization data from the two operational RTLs (UWB and CV) deployed in our industrial research lab, the AAU 5G Smart Production Lab. [46], with the aim of integrating the outputs in our digital twin framework for data simulation/prediction/synthesis. In the following we describe the physical experimental setup, the realistic operational test conditions, as well as the data processing and modeling approaches.

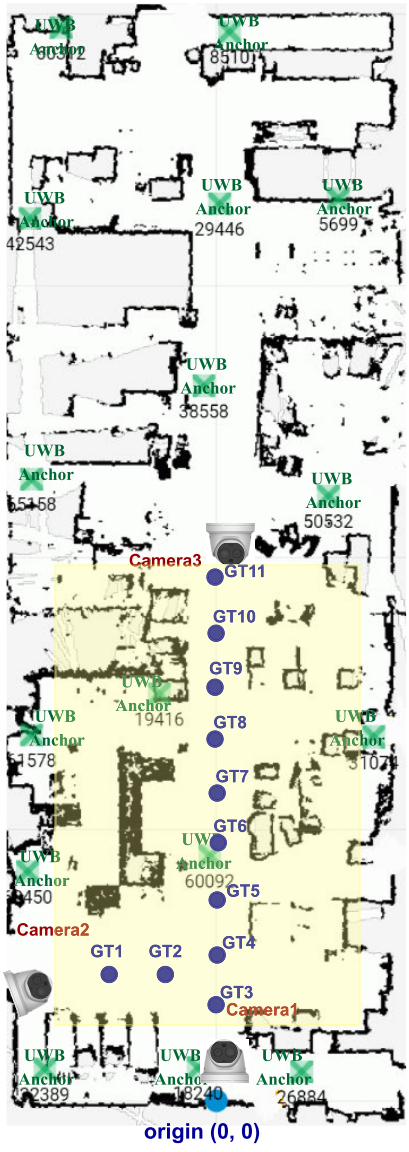

FIGURE 2. Layout of the main hall of the AAU 5G Smart Production Lab, illustrating the position of the indoor RTLS deployments (UWB: green crosses, CV: camera icons), as well as the target key production area (yellow rectangle) and the reference GT points (blue dots).

A. REALISTIC INDUSTRIAL TESTBED AND OPERATIONAL INDOOR RTLS DEPLOYMENTS

The experimentation took place in the main hall of the AAU 5G Smart Production lab, which is a small realistic factory hall of 14 m × 40 m, equipped with production lines, robotic cells, AMRs and other industrial automation equipment. Here, a key production area of 12 m × 20 m was defined around a production line, as this is a corridor-intersection traffic-intense area where mobile robots and human workers typically coexist and, therefore, efficiency and safety enhancements are of importance [48]. This target area is highlighted in yellow in Fig. 2 over the factory hall layout.

TABLE 1. Comparative overview of indoor positioning systems utilizing UWB, CV, and their integration across various studies.

RTLS	UWB					CV			UWB & CV		
Ref.	**[15]**	**[19]**	**[20]**	**[21]**	**[23]**	**[35]**	**[44]**	**[45]**	**[30]**	**[47]**	**This Work**
UWB Anchors #	8	4	3	4/8	6	NA	NA	NA	3	4, 10	16
UWB Radio Chip-Set	DecaWave DW1000	DecaWave DW1000	DecaWave DW1000	DecaWave DW1000	DecaWave DW1000	NA	NA	NA	Unknown	Samsung UM100	DecaWave DW1000
Cameras[1]#	NA	NA	NA	NA	NA	5	6	3	1	1	3
Camera Fusion	NA	NA	NA	NA	NA	Post-processing[2]	Post-Processing[2]	Post-Processing	NA	NA	Post-Processing
Environment	Indoor, Industrial	Indoor, Non-Industrial	Indoor & Outdoor, Non-Industrial	Indoor, Industrial[3]	Indoor & Outdoor, Non-Industrial	Simulated, Indoor, Industrial	Indoor, Non-Industrial	Indoor, Non-Industrial	Indoor, Non-Industrial	Indoor, Non-Industrial	Indoor, Industrial
Room Area [m^2]	560	78	24, 229	80	-	-	-	-	-	560	
Subject	Tripod & mobile robot	Tripod & human	human	human	Tripod[4]	human	human	human	human	human	Tripod & human
Measurement Scenarios	Mobile & Static	Mobile & Static	Mobile & Static	Mobile	Static	Mobile	Mobile	Mobile	Mobile	Mobile	Mobile & Static
Sample Rate [Hz]	50	3.57	3.57	23 (8 anchors), 11.5 (4 anchors)	3.3	4	-	10	-	5 (UWB), 10 (CV)	50 (UWB), 25 (CV)
Samples #	815-830 k (static), 100 k (mobile)	2.8 k(static), - (mobile)	37 k(static), 178, 353 (mobile)	6.2 K, 12.5 k	36.6 k	320-640	12.4 k	-	-	9.3 k	6.5 k, 6.7 k (UWB, static), 2.5 k (CV, static), 2.4 K (UWB, mobile), 936 (CV, mobile)
GT Points #	72	26	4, 5	-	61	-	-	-	-	-	11
RTLS Accuracy [cm]	median$\leq$20	median$\leq$255	mean$\leq$39.9	median$\leq$32	median$\leq$18	mean$\leq$60	mean$\leq$40	mean$\leq$22	mean$\leq$34 (UWB), mean$\leq$30 (CV), mean$\leq$25 (CV & UWB)	RMSE$\leq$32 (UWB), RMSE$\leq$18 (CV & UWB)	median$\leq$23 (UWB), median$\leq$25 (CV)
Model	NA	Gaussian + Gamma	Gaussian + Gamma	bank of Gaussian mixtures	Gaussian + Gamma	NA	NA	NA	NA	NA	Gamma
Model Accuracy [cm]	NA	-	-	-	-	NA	NA	NA	NA	NA	$\leq$6 (90%)

[1] All the cameras in these studies were of RGB type.
[2] The camera fusion algorithm requires knowledge of camera position/model.
[3] Measurements were performed in open space area.
[4] A human was walking around as a source of NLOS situation.

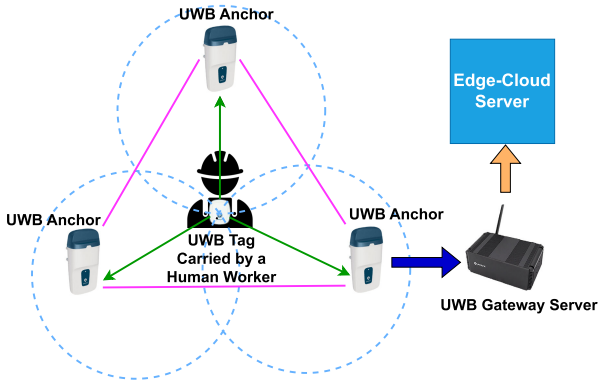

FIGURE 3. UWB RTLS data processing flow, including trilateration between end devices (tags) and infrastructure nodes (anchors), and centralized processing and storage at gateway server.

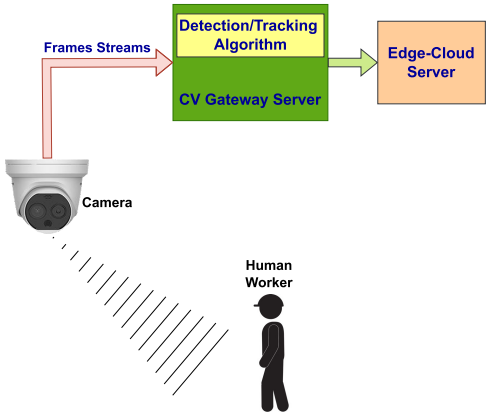

FIGURE 4. CV RTLS data processing flow, including video detection by the infrastructure elements (cameras), and centralized data processing at gateway server.

As also described in the figure, the lab is equipped with an UWB positioning system based on 16 anchors deployed at 5-6 m height, close to ceiling level (green crosses in the figure), and a CV-based system composed of 3 cameras (camera icons in the figure) which are constantly monitoring from aerial next-to-the-ceiling positions the target shop-floor aisles around the production line. The figure also displays the 11 ground truth (GT) points (blue dots in the figure) that were selected for positioning performance evaluation over the key production area. These points were marked on the floor, with an inter-point distance of approximately 2 m, to obtain relevant statistics spanning over the whole main aisle intersection at the key production area. These reference points were measured with mm accuracy using a total station theodolite [49]. Both positioning systems were configured and calibrated to the same Cartesian coordinate system with origin (0,0) position located in the south wall of the research lab as indicated in Fig. 2. Physically, this reference position corresponds an wall-installed charger device for industrial AMRs.

1) UWB RTLS

UWB RTLSs are typically based on battery-powered transmitters (tag) deployed over the localization targets that emit short-duration UWB RF pulses, and also multiple receivers (anchors or reference nodes) which are strategically placed at known locations throughout the environment. The operational UWB RTLS deployed in our factory hall was an industrial-grade system based on enterprise anchors by pozyx [50]. Prior to operation, the system was fully-calibrated in the horizontal domain (information about exact anchor 3D position with mm precision is logged by the system and combined with its own auto-over-the-air calibration routines). The UWB transceiver (tag) deployed for measurement and evaluation was based on commercial DecaWave DW1000 equipment [51]. The UWB RF positioning signal was configured as per the following settings: UWB channel 2 (3774-4243.2 MHz), 500 MHz bandwidth (enabling a timing resolution of 1.6 ns), data rate of 110 kbps, a preamble length of 1024 bits, a pulse repetition frequency of 64 MHz, and a transmission power of 20 dBm. The update rate of the transceiver (tag) was set to 50 Hz. The 2D localization data from the UWB RTLS is collected from an edge-cloud system gateway/controller through Message Queue Telemetry Transport (MQTT) communication protocol [52]. In our case, positioning estimates of each tagged object or individual are obtained in real time at a rate of 50 Hz positioning measurements per second by combining trilateration results based on time-difference-of-arrival (TDoA) from multiple anchors. Each UWB tag is associated with an individual ID within the system, ensuring precise identification and discrimination between different tagged objects or individuals. The overall data flow for the UWB RTLS is briefly summarized in Fig. 3.

2) CV RTLS

The second RTLS deployed in our industrial research lab utilizes surveillance thermal/RGB cameras [53], complemented by a customized real-time deep learning person detection/tracking algorithm by Ambolt AI [54]. This algorithm outputs updated floor-mapped 2D coordinates of the target elements (humans) based on YOLOv4 detection with bounding boxes as the key component [55]. The cameras were mounted in next-to-ceiling locations in such a way to cover the whole key production area, to make sure that a human worker can always be detected and tracked by, at least, one camera. The frame update rate of cameras is 25 fps, i.e., positions received from the CV system update approximately every 40 ms. The frames stream are fetched by a local server/gateway to be processed and then sent to an edge-cloud server as depicted in Fig. 4. As in the UWB case, MQTT is used to collect CV localization data, discriminating the different detected human workers with different unique IDs, from the edge-cloud server.

a: MULTI-CAMERA INTEGRATION FOR OPTIMIZED DETECTION

The surveillance cameras operate as three separate systems. When a person is detected by multiple cameras in the CV

Algorithm 1 Best Camera Selection Algorithm

Input: $C \leftarrow \{c_1, c_2, \ldots, c_N\}, R \leftarrow \{r_1, r_2, \ldots, r_N\}$
Output: c_{best}
$K \leftarrow$ non-zero$(C \times R) \leftarrow \{k_1, k_2, \ldots, k_M\}, M < N$
$S \leftarrow \{s_1, s_2\} \leftarrow$ SortAscending$(K, d_{CV,avg}(\cdot), 1:2)$
BEST CAMERA Selection
if $\left\{\left(\frac{d_{CV,avg}(s_2)}{d_{CV,avg}(s_1)} < 1.3\right)\right.$ **and** $\left.\left(\frac{d_{CV,SD}(s_2)}{d_{CV,SD}(s_1)} < 1\right)\right\}$ **or** $\left\{\left(\frac{d_{CV,var}(s_2)}{d_{CV,var}(s_1)} < 1.7\right)\right.$ **and** $\left.\left(\frac{numel(s_2)}{numel(s_1)} > 5\right)\right\}$ **then**
  $c_{best} \leftarrow s_2$
else
  $c_{best} \leftarrow s_1$
end if
return c_{best}

system, each camera provides a distinct coordinate for that person. To optimize the performance of the CV system and integrate all three cameras effectively, we defined confidence regions for each camera. These confidence regions are calibrated and encompass the output estimated coordinates of the human that are considered as correct, considering NLOS regions, potential angular and range degradation due to the type of aperture and lens used in the camera [56].

Thereafter, an integration algorithm was developed by taking into account the confidence regions and statistical measures of the cameras, to fuse and optimize their localization data into a single and more accurate and robust final position for each detected individual. The considered statistical measures are: mean accuracy ($d_{CV,avg}$), standard deviation ($d_{CV,SD}$), and the number of samples (*numel*) output by each camera in a given time period. The general formulation is given in Algorithm 1 and aims at selecting the best camera (c_{best}) based on the full set of N available camera interfaces (C) and the corresponding confidence regions masks (R). First, the full set of cameras with available information is filtered by the confidence region masks, identifying the group of $M < N$ camera interfaces with possible correct detection (K). Next, these interfaces are sorted in ascending order as per their mean accuracy, and the two cameras with the best accuracy (s_1, s_2) are selected as best camera candidates. Subsequently, the best camera selection is done by evaluating a number of conditions comparing the performance of each of the candidate camera interfaces. Generally, the best camera is the one with highest accuracy, e.g., s_1. However, in some cases, the mean accuracy computation over a given interval of time can be biased by the number of run-time available samples, impacting also the standard deviation of the calculation and, therefore, an empirical check of the robustness of the detection is implemented. If the mean accuracy of second interface is less than 30% worse than the one from the first interface, and its standard deviation is lower than the one from the first interface, then s_2 is chosen as best camera, despite having a lower mean accuracy. This is also the choice if the number of detection samples of the second interface is more than 5 times larger than the one from the first interface and still the second interface accuracy is not less than 70% worse than the one from the first interface. The first condition discriminates the correctness of the detection with cameras with a similar performance, typically, in areas with a similar distance and angular conditions between the camera and the human target. The second condition filters out those cases where a camera in not the best distance and angular conditions performs sporadic lucky detections, which are typically appearing and vanishing rapidly and not constant in time, which leads to a clearly lower number of samples as compared to the one from a camera in good detection conditions. Thus, the second-best camera, which demonstrates a higher detection success rate with acceptable accuracy variance, is selected, prioritizing reliable detection in industrial settings. The proposed algorithm for integrating multiple camera outputs has a complexity order of approximately $O(M \log M)$, suggesting a low computational demand. This characteristic makes it a suitable solution for our target real-time application.

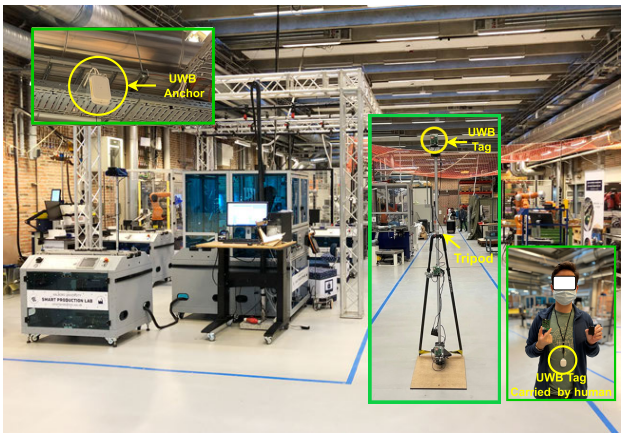

FIGURE 5. UWB measurement setup illustrating the location of the elevated wall-mounted anchors, tag tripod setup for non-human reference, and the on-human tag setup for operational evaluation.

It should be noted that, our realistic industrial research lab scenario, implements $N = 3$ camera interfaces to monitor the key production area. As displayed in Fig. 2, the cameras are strategically deployed so that the shop-floor aisles are always in sight from two of the cameras. This facilitates the definition of the confidence regions, which always guarantees that the initial down-selection is done to $M = 2$ camera interfaces, and direct evaluation of the best camera selection conditions is possible. The specific choices of confidence regions will be further elaborated in Section IV-B. Similar deployment strategies are foreseen in real factory scenarios, as the layouts are typically alike, which ensures that our algorithm will be valid in those cases as well without loss of generality.

B. MEASUREMENT SETUP, TEST CONFIGURATIONS, AND DATA PROCESSING PROCEDURES

The evaluation of the two selected RTLSs considered both static and mobile human operational conditions. The static

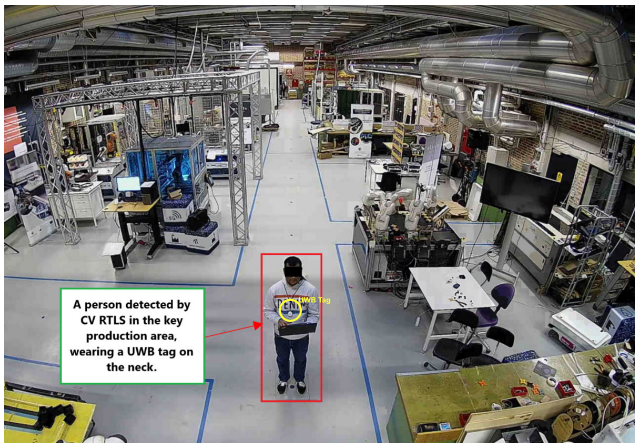

FIGURE 6. A frame captured by the ceiling-mounted camera 1, illustrating the output of the CV system with one person detected over the GT3 reference point.

condition was evaluated with a human standing at the different GT reference positions, while the mobile condition was evaluated with a human walking over the route defined by the different GT reference points. In the UWB case, the static evaluation was performed with a tag carried by a human in a string around the neck. This is displayed in Fig. 5. The height of the tag on the human was approximately 1.25 m above ground floor. The figure also describes an alternative setup for the static UWB case where the tag was mounted on a tripod at 1.98 m height. This alternative setup was used to collect measurements to compare with the human case and investigate the effect of the human on the accuracy of the RF localization system in industrial settings. For the CV case, no tag or any other hardware was needed, as the human position detection is automatically done based on video processing. Fig. 6 illustrates a frame captured by one of the cameras, with a detected person over GT1 in the red bounding box.

Under these settings, and considering the calibrated GT points as a reference as illustrated in Fig. 7, the 2D Euclidean distance (d) was calculated from the (X, Y) RTLS samples as Eq. 1 and Eq. 2 to measure the accuracy of the UWB and the CV systems, respectively.

$$d_{UWB} = \sqrt{(X_{UWB} - X_{GT})^2 + (Y_{UWB} - Y_{GT})^2} \quad (1)$$

$$d_{CV} = \sqrt{(X_{CV} - X_{GT})^2 + (Y_{CV} - Y_{GT})^2} \quad (2)$$

While the applicability of Eqs. 1 and 2 is trivial for the static case, where there is a one-to-one correspondence between UWB/CV positioning samples and GT reference points; in the mobile case, the human individual target moves along the 19 m route path between GT1 and GT11, twice (in forth and back directions) and, therefore, synchronization/alignment of the UWB/CV measurements to the GT points route over time is needed. To do this, a mobile reference paths was derived by aligning the real-time measurement to the mobile route GT points, and interpolating GT positions, at time stamps matching the CV/UWB data time stamps, as detailed in Fig. 8. The

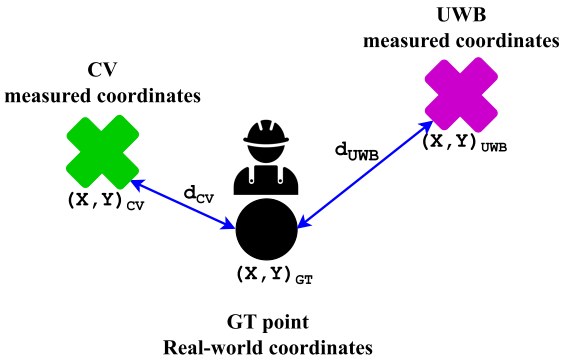

FIGURE 7. Description of the computation of the 2D Euclidean distance based on the coordinates obtained from the UWB/CV RTLSs and the real-world GT reference coordinates of a given human worker.

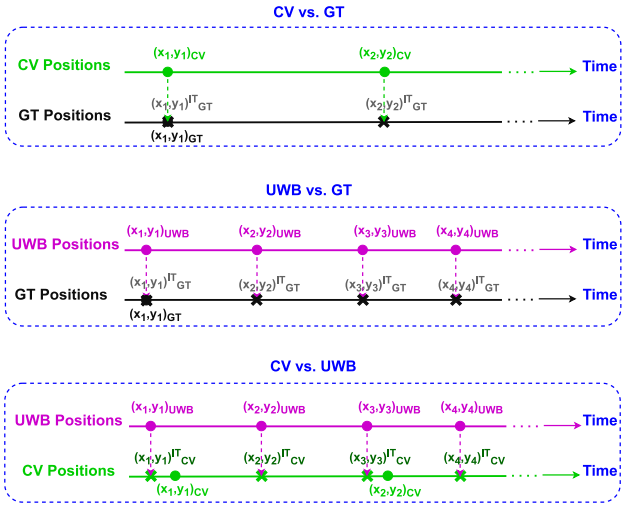

FIGURE 8. Description of the measurement synchronization approach for the mobile case, considering interpolation of GT samples according to CV/UWB data time stamps (CV and UWB vs. GT), and upsampling of the CV measurements to match the UWB data (CV vs. UWB); with circles and crosses representing measured and interpolated data, respectively.

individual UWB/CV operational accuracy performance was analyzed independently. However, additional analyses based on concurrent measurements both in static and mobile cases were performed to benchmark simultaneous UWB and CV RTLS performance, in order to be able to establish potential run-time safety measures for detecting humans without tags. In this case, the explored metric (Δ) was the Euclidean distance between the simultaneous UWB and CV positioning data, as described in Eq. 3. In static case, Δ is computed as the Euclidean distance between the average of all recorded CV samples and the average of all recorded UWB samples at each GT point; whereas in mobile case, to compute Δ, the CV samples were interpolated to match the UWB samples time-wise, as also described in Fig. 8.

$$\Delta = \sqrt{(X_{CV} - X_{UWB})^2 + (Y_{CV} - Y_{UWB})^2} \quad (3)$$

In the static case, 6509, 6774, 2496 measurement samples were collected for the UWB (tag on tripod), UWB (tag on human), and CV RTLSs, respectively, at each GT position.

The number of samples was larger for the UWB RTLS evaluation, as this system has a higher acquisition rate configured. All samples are used in the statistical analysis to guarantee a fair comparison of the performance over a similar operational time period of around 120 s. For the mobile case, the 19 m route between GT1 and GT11 was walked twice, in opposite directions, ensuring variable operational conditions. The total number of samples collected over the route was 2406 and 936 for the UWB and CV RTLSs, respectively, with an average route traverse time of around 40 s (average walking speed of 1 m/s $\approx$ 3.6 km/h). The discrepancy in the number of captured CV samples vs. the expected one based on the duration and sampling rate is attributed to two factors: first, the detection algorithm's occasional failure to identify a person in the captured frames, and second, for consistency and fair comparison, we standardized the sample count across all GT points to match that of GT11, which had the lowest count due to the relative position of this GT point to camera 3. The effective number of CV synchronized samples for comparison, as per the interpolated upsampling procedure described in Fig. 8 was, therefore, 2406.

C. ESTIMATED ERROR DISTRIBUTION MODEL

One of the main contributions of this study is the modeling of the measured localization inaccuracies for the UWB and CV RTLSs within our operational industrial environment. Our ultimate goal is to employ these models for data simulation/estimation/synthesis within the context of a digital twin framework, which in turn facilitates making informed decisions, leading to notable enhancements in production processes and precise robot path planning.

To model the positioning error across different configurations, we chose the Gamma distribution (see Eq. 4) for its versatility and its ability to approximate a wide range of asymmetric and skewed distributions. While some studies in the reviewed literature used low-sigma Gaussian distributions, primarily in scenarios with clear LOS conditions, or a combination of Gaussian (for LOS) and Gamma (for NLOS) distributions [19], [23], the right-skewed nature of our experimental data justified the choice of the Gamma distribution. This skewness is attributed to factors such as Euclidean distance, NLOS conditions, and inherent noise in industrial environments. Our approach was carefully designed to maintain model independence from predefined parameters or specific configurations, enhancing its adaptability. This design ensures the model is straightforward to interpret and apply, facilitating insights into data inaccuracy behaviors and its application in various industrial settings.

$$s = \frac{1}{\Gamma(\alpha)\beta^{\alpha}} x^{\alpha-1} e^{-\frac{x}{\beta}} \tag{4}$$

Where:

$$\Gamma(\alpha) = \int_0^{\infty} t^{\alpha-1} e^{-t} dt$$

In Eq. 4, x represents the random variable, α is the shape parameter, β is the scale parameter, and $\Gamma(\alpha)$ is the gamma function evaluated at α. The mean and variance of the gamma distribution respectively are $\mu = \alpha\beta$ and $\sigma^2 = \alpha\beta^2$. These parameters are estimated using maximum likelihood estimation (MLE) algorithm [57] for each experimentally measured data. To better characterize the estimated distribution, we also measured its skewness (S) as Eq. 5.

$$S = \frac{E(x-\mu)^3}{\sigma^3} \tag{5}$$

where μ is the mean of x, and $E(t)$ represented the expected value of t. Skewness is a statistical measure that quantifies the asymmetry of data relative to the sample mean. When skewness is negative, it indicates that the data is more spread out to the left of the mean than to the right. Conversely, when skewness is positive, it suggests that the data is more spread out to the right of the mean [58]. We also calculated the goodness of fit (GOF) for each estimated distribution, i.e. the error norm between the experimental and estimated CDF using mean square error (MSE) as the cost function [59]. A zero goodness of fit indicates a perfect fit of experimental data to the estimated distribution. The estimated values of α, β, along with the calculated S and GOF for each estimated distribution are presented in IV-C3, along with the model analysis.

IV. RESULTS

This section describes the results in perspective of the different objectives and contributions set for this study. First, results for the analysis of the human impact on operational UWB positioning performance are discussed. Next, the impact of integration and optimization of CV localization data from multiple surveillance cameras is addressed. Later, the individual operational positioning performance results are presented and compared for the UWB and CV RTLSs along with the estimated empirical error models for both static and mobile conditions. Finally, the safety measure for detecting humans without UWB tags is introduced based on the simultaneous evaluation of the UWB and CV RTLs.

A. IMPACT OF THE HUMAN BODY ON UWB POSITIONING IN INDUSTRIAL SETTINGS

Fig. 9 displays the raw measurement results obtained with the tripod setup at the different GT positions for the static case. As shown, the UWB localization for a given position is accurate, as there are no large deviations of the raw measurement data from the GT reference points. In this non-human tripod case, the UWB localization is also stable, as the dispersion of the raw measurement data around the GT reference points is low. As a reference, by analyzing the statistics of d_{UWB} over the full data set, a median accuracy of 12 cm and a standard deviation of 4 cm was observed. In contrast, the raw measurement data presented in Fig. 10 for the case where the UWB tag was

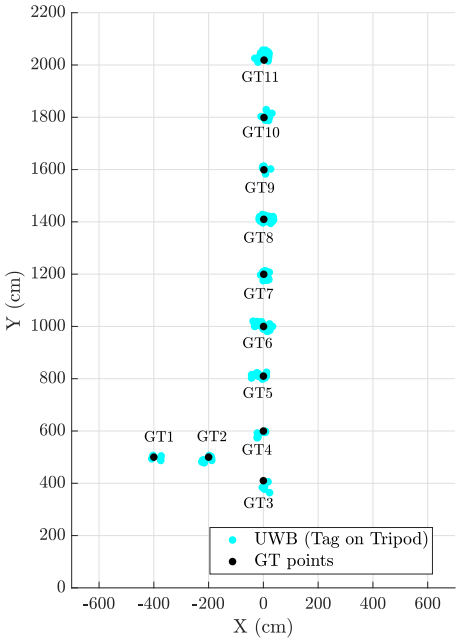

FIGURE 9. Raw UWB positioning measurement data for the tripod setup in static conditions.

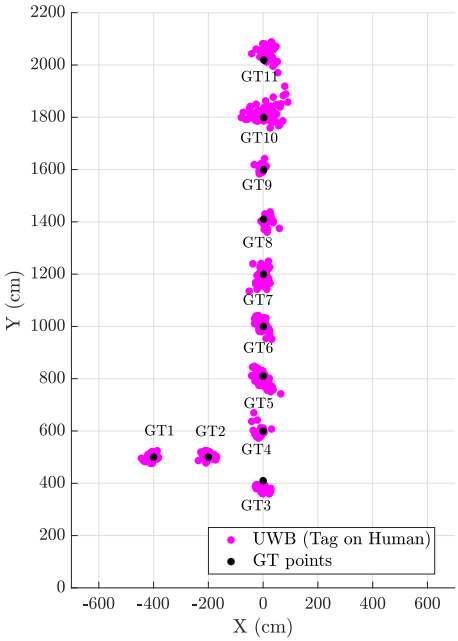

FIGURE 10. Raw UWB positioning measurement data for the tag-on-human setup in static conditions.

placed on the human exhibits some deviations from the GT points in some cases (especially around GT8) and a larger variability as compared to the non-human tripod setup. In this case, the median accuracy was found to be 19 cm with a standard deviation of 14 cm. This indicates that, in the considered experimental settings, the human body introduces a degradation of approximately 5 cm in the UWB positioning performance, and increases the uncertainty of the system by a factor of 3.5. The cause of this is clear, as the results involving the human are influenced by the shadowing induced by the body, which obstructs, reflects, or scatters the UWB radio signals, leading to reduced strength or delayed arrival, which consequently introduces errors in the UWB ranging estimation by the operational UWB locating system.

It should be noted that this study explores the impact human shadowing on the self-positioning. However, the conclusions drawn from the examination of a single tagged subject can be extended to scenarios involving multiple individuals within the work area if they are not very close to each other (which is a fair assumption for key operational production areas). Moreover, the impact of human workers standing next to each other is expected to be minimal, as the anchor density of the considered deployment should guarantee enough links even in the presence of some extra blockage.

In [19] and [20], the best UWB accuracy reported for an non-industrial scenario was 20 cm, with an standard deviation of 10 cm for UWB tags deployed in the forehead of a human person. For tags deployed over the chest (as it is our case), the same study reported an accuracy in the order of 246 cm, with high variability of up to 166 cm of standard deviation. Other studies, which even considered enhanced processing algorithms accounting for spatial and angular deployment information [20], [22], described median accuracies in the order of 20-50 cm. According to this, even in the presence of human shadowing, the precision of UWB positioning in our operational industrial scenario is comparable to that reported in non-industrial scenarios. Despite the difference in clutter nature and dimensions of the industrial and non-industrial scenarios, the density of the deployment is typically larger in industrial scenarios, which increases the LOS probability in the UWB transmissions, reducing the potential distortion induced by the large metal obstacles in the radio propagation, and thus, leading to a comparable reference accuracy, even in the presence of human shadowing.

B. OPTIMIZED CV LOCALIZATION BY MULTI-CAMERA INTEGRATION

Fig. 11 illustrates the human localization errors (d_{CV}), based on the individual processing of the raw measurement data, for each camera at each GT position (orange dots for camera 1, blue dots for camera 2, and red dots for camera 3). As depicted, these errors are quite variable as they depend on the angular and distance conditions of the GT position towards the specific camera placements. When the GT points are in good field of view conditions, the CV localization error ranges consistently from 1 to approximately 20 cm. In bad conditions, the CV positioning error for the individual cameras is increased to up to 0.5-10 m. It should be noted that there are GT points that fall outside the field of view of specific cameras and, therefore, no data is available at that particular position.

This emphasized the importance of considering the spatial coverage characteristics of individual cameras, and motivated the definition of confidence regions associated to the different cameras, as described in Section III-A2. In our case, the

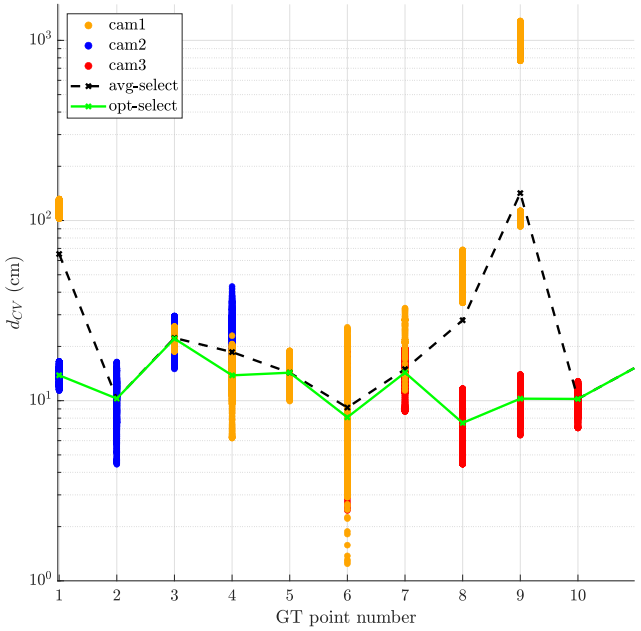

FIGURE 11. CV positioning performance: individual camera accuracy and output of the selection algorithms for each of the GT points.

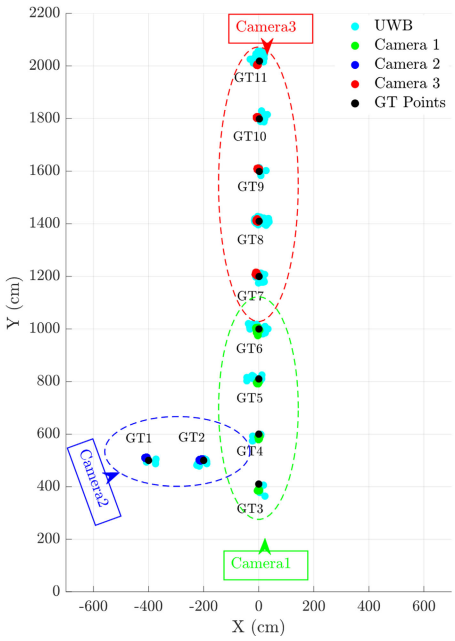

FIGURE 12. CV positioning data as per the best camera selection algorithm in static conditions including confidence regions for each of the cameras.

confidence region for camera 1 spans over GT points 3-6. For camera 2, the confidence region encompasses the areas around GT points 1 and 2. The rest of the GT points 7-11 are associated to the confidence region for camera 3. To better understand the angular and distance camera conditions in each of the regions, Fig. 12 can be used as a reference. The approximate confidence regions are illustrated by the dashed ellipses for each of the cameras. Remember that in our setup, the cameras are strategically placed so that each of the two perpendicular target aisles in our key production are are covered by at least two cameras. Effectively, the best camera, the one dominant over each of the defined confidence regions, is that with short distance and target angular relation close the camera boresight direction. For further reference, in respect to the camera inaccuracies across the different GT points, Table 2 provides information about the relative Euclidean distances and elevation/azimuth angles of each camera with respect to each GT point. As depicted in Figures 2 and 12, camera 2 is slightly tilted, which explains why GT9 remains visible to this camera. However, the production line creates a NLOS condition for GT5 through GT8 for camera 2. GT11 is positioned directly beneath camera 3 and is only within the field of view of this camera, which accounts for the large error observed at this GT point.

Having such CV output performance information allowed us to develop the best camera selection algorithm to select the appropriate human location reading from the CV RTLs, even in the presence of multiple detections in the different cameras. Fig. 11 further demonstrates the effectiveness of our proposed method in enhancing accuracy through the integrated evaluation of readings from the three independent cameras according to their related confidence regions (solid green line) by comparing its performance with a baseline selection method based on direct averaging of the human target readings at the different cameras, without considering any field of view quality conditions (dashed black line). For our proposed best camera selection algorithm, the average, median, and maximum localization errors are 12 cm, 13 cm, and 26 cm, respectively. In comparison, these values for the baseline method are 32 cm, 15 cm, and 142 cm. This implies that, on average, our integration algorithm outperforms the baseline method by 60%.

When compared to the works in the literature, [44] reported an average accuracy of 40 cm, requiring the camera model for data fusion, and only working with two cameras. The authors in [45] employed three fusion methods: one with uniform weighting resulting in an average error of 22 cm, another selecting the best camera for accuracy with an average error of 21 cm, and the third using error bias weighting which assigns higher weights to cameras with higher accuracy, resulting in an average accuracy of 18 cm. The weakness of their first method is the loss of the benefits of more accurate cameras, while the weakness of the latter two methods is relying on just one statistical measure of average accuracy, which is not robust. Therefore, our best camera selection algorithm shows a great potential, at expense of the requirement of prior calibration knowledge (confidence regions), which should be easy to obtain in operational industrial scenarios.

Apart from the information about the confidence regions selected for each of the three cameras, Fig. 12 displays the CV positioning data obtained as an output of the best camera selection method with a human operator standing at each of the GT points for the different cameras. In general, the performance is stable and the dispersion of the CV data

TABLE 2. Cameras Euclidean distances along with their elevation and azimuth angles with respect to each GT point.

	Camera 1			Camera 2			Camera 3		
	Distance [m]	Elevation Angle [°]	Azimuth Angle [°]	Distance [m]	Elevation Angle [°]	Azimuth Angle [°]	Distance [m]	Elevation Angle [°]	Azimuth Angle [°]
GT1	7.60	41.12	135.71	7.18	38.83	10.30	18.05	19.41	255.72
GT2	6.74	47.90	117.70	8.80	30.74	7.59	17.69	19.82	262.41
GT3	5.88	58.19	91.85	10.51	25.34	0.60	18.41	19.02	269.34
GT4	7.07	44.99	91.15	10.70	24.87	11.89	16.62	21.16	269.26
GT5	8.68	35.15	90.81	11.28	23.50	23.34	14.68	24.12	269.14
GT6	10.30	29.05	90.64	12.10	21.83	32.28	12.97	27.55	269.00
GT7	12.08	24.44	90.52	13.21	19.92	40.10	11.24	32.27	268.79
GT8	14.02	20.89	90.44	14.58	17.98	46.75	9.53	39.03	268.45
GT9	15.81	18.43	90.38	15.95	16.38	51.63	8.14	47.47	267.92
GT10	17.72	16.39	90.34	17.51	14.89	55.84	6.95	59.70	266.73
GT11	19.84	14.60	90.30	19.31	13.47	59.61	6.14	77.64	261.25

around the GT reference points is lower than for the UWB RTLS. This is observed from the median accuracy (12 cm), and standard deviation (4 cm) of the integrated CV RTLs, which are lower that those experienced in the UWB case.

C. OVERALL REAL-TIME LOCALIZATION ACCURACY AND ESTIMATED PERFORMANCE MODELS

After exploring briefly the impact of the human body on the UWB positioning in the industrial scenario and the performance of our optimized CV system in static human conditions, this section takes a closer statistical look to the results and compares in detail the performance of the UWB and CV RTLSs in both static and mobile conditions. The statistical accuracy results for the different configurations are further modeled by Gamma distributions (as explained in Section III-C), and discussed in terms of precision at different confidence levels.

1) PERFORMANCE IN STATIC CONDITIONS

Fig. 13 displays the empirical complementary distribution functions (CDFs) of the positioning performance (localization errors) for the UWB (d_{UWB}) and CV (d_{CV}) RTLSs in static human conditions (solid lines), as well as the ones from their associated Gamma models (dashed lines). As depicted, in static conditions, the CV performance is more robust than the UWB one in either the tripod or the on-human setup. At medial level, the CV localization error is 12 cm. This is increased by 1 cm for the UWB tripod case, and by 7 cm for the UWB on-human case. For UWB, these differences are further increased to 25 and 117 cm at maximum level, for the tripod and on-human setup, respectively, for a maximum reference CV localization error of 26 cm. While these are considered the most relevant accuracy indicators, it should be noted that in 10% of the cases, the UWB RTLS with on-human tag setup performed better than the optimized CV one. A summary of key performance statics is given in Table 3 for the different configurations.

In comparison to our previous study, reported in [15], where the UWB deployment in the same industrial operational scenario considered only 8 infrastructure anchors (half than in this study), the UWB positioning performance has now improved. While the median accuracy performance is similar, the maximum ranging error is reduced by a factor of 2. It is worth noting that these improvements were achieved in a median industrial cluttered environment, without applying any optimization techniques, only densifying the anchor deployment.

2) PERFORMANCE IN MOBILE CONDITIONS

Fig. 14 displays the empirical complementary distribution functions (CDFs) of the positioning performance (localization errors) for the UWB (d_{UWB}) and CV (d_{CV}) RTLSs in mobile human conditions (solid lines), as well as the ones from their associated Gamma models (dashed lines). Differently from the static case, if the human operator moves, the UWB RTLS performs better than the CV one. In this case, the median and maximum localization accuracy values for UWB with the on-human tag setup are 23 and 80 cm, respectively. The localization error is slightly higher for the optimized CV setup, where a median error of 25 cm and a maximum error of 89 cm. As for the static case, the key performance statistics are summarized in Table 3.

As a further reference, in Fig.15, the spatial localization data is compared for both RTLs. Despite the previous statistical differences, as displayed, both the UWB and CV RTLs are able to track the path followed by the human. From these results, we can conclude that in operational mobile conditions, the median accuracy of UWB exhibited minimal degradation, establishing it as a reliable RTLS choice. In contrast, the CV system demonstrated more pronounced accuracy deterioration, which can be attributed to

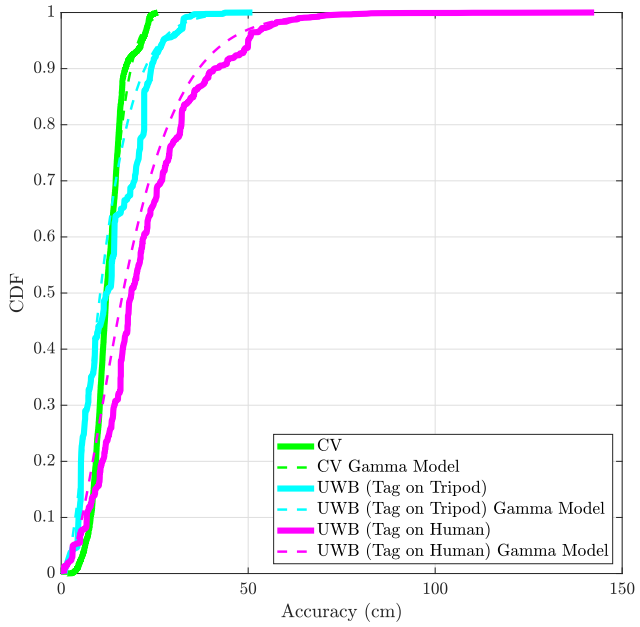

FIGURE 13. CDF of the human detection accuracy of the UWB (tag on tripod/on-human) and CV RTLSs in static conditions.

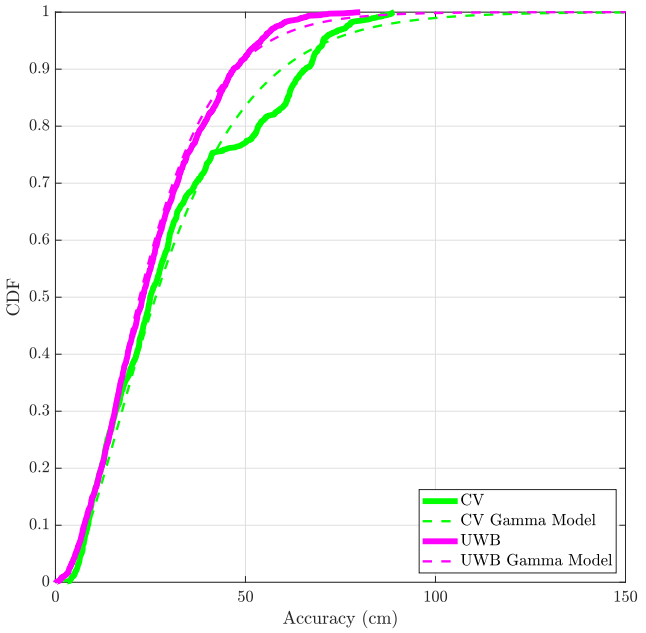

FIGURE 14. CDF of the human detection accuracy of the UWB (on-human) and CV RTLSs in walking mobile conditions.

the decreased performance of tracking algorithms, especially when the human target is in motion, leading to distortions in the CV-based measurements. The reduced maximum error observed in the UWB mobile scenario as compared to the static case can be attributed to the diminished influence of regions subjected to increased degrees of shadowing. The main differences are observed by comparing Figs. 10 and 15 in the areas around GT3 and GT4, and GT10 and GT11. At those positions, for the UWB mobile case, the orientation of the human while walking over the measurement route is optimized (from a radio shadowing perspective) as compared to the standing cases explored at the same positions during the static UWB assessment.

3) ESTIMATED PERFORMANCE MODELS

The observed performance of the UWB and CV RTLSs in terms of statistical distributions of accuracy/localization error was modeled using Gamma distributions. Table 4 reports the Gamma distribution parameters, skewness, and goodness of fit for each estimated distribution. The statistical outputs of these models are demonstrated in Figs. 13 and 14, to illustrate their fits to the empirical error localization distributions previously discussed for the different scenarios.

Previous studies [19], [20], [24] considered a mixture of Gaussian and Gamma distributions respectively for LOS and NLOS conditions to model human localization error data. However, in our work, which is an operational industrial setup (with extensive NLOS, reflections, and noises) contrary to their non-industrial settings, the Gamma distribution effect is more pronounced. This was especially evident in the case of the UWB tag carried by a human, where human body played a dominant role in shadowing phenomena. The larger and more disperse localization errors measured in this case are obvious

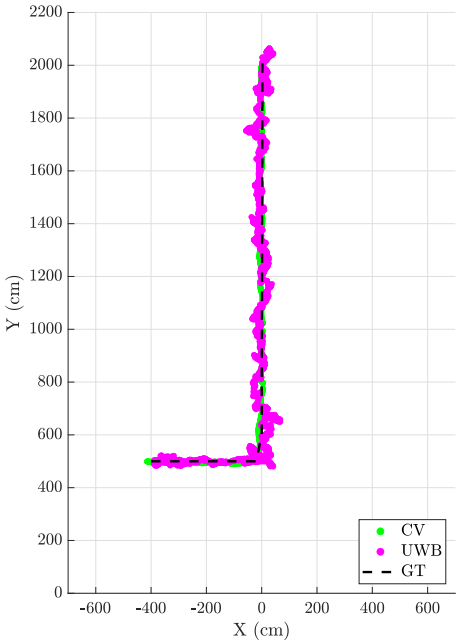

FIGURE 15. Raw UWB positioning measurement data for the tag-on-human setup and CV positioning data as per the best camera selection algorithm in mobile conditions. The GT route is displayed on top as a reference.

in Fig. 10 (highlighting data dispersion) and Fig. 13 (showing a heavy-tailed CDF), which in turn resulted in larger β values (and subsequently S) of the corresponding estimated Gamma model, with similar α. In the UWB RTLS case, the estimated Gamma models for both static and mobile measurements, exhibit a similar degree of asymmetry (S). However, in the mobile case, the greater variability in the data implies higher α and β values, potentially due to the challenges introduced

TABLE 3. Summary of key accuracy performance statistics for the UWB and CV RTLSs for human detection in operational conditions.

	Static Scenario			Mobile Scenario		Run-time Safety (CV vs. UWB)	
	CV	UWB (tripod)	UWB (human)	CV	UWB	static case	mobile case
Average [cm]	13	14	22	31	25	17	41
Std. Dev. [cm]	4	8	14	21	15	13	20
Median [cm]	12	13	19	25	23	13	38
Maximum [cm]	26	51	143	89	80	52	97

TABLE 4. Parameters of the human localization error models estimated as Gamma distributions for the UWB and CV RTLSs in operational conditions.

	Static Scenario			Mobile Scenario		Run-time Safety (CV vs. UWB)	
	CV	UWB (tripod)	UWB (human)	CV	UWB	static case	mobile case
α	8.88	2.44	2.20	2.13	2.46	3.01	3.42
β	1.45	4.93	8.80	14.58	10.34	5.53	11.97
S	0.68	1.21	1.34	1.35	1.30	1.14	1.09
GOF	6.3×10^{-4}	5.4×10^{-3}	4.8×10^{-3}	9.9×10^{-4}	2.2×10^{-4}	1.4×10^{-2}	6.0×10^{-4}

TABLE 5. Evaluation of the human localization error model outputs at 90% and 99% confidence levels for the UWB and CV RTLSs in operational conditions.

		Static Scenario			Mobile Scenario		Run-time Safety (CV vs. UWB)	
		CV	UWB (tripod)	UWB (human)	CV	UWB	static case	mobile case
99.9%	Experimental [cm]	25	41	93	89	79	52	95
	Estimated [cm]	31	50	85	139	106	63	144
	Deviation [cm]	6	9	-8	50	27	11	49
90%	Experimental [cm]	17	24	41	66	47	23	68
	Estimated [cm]	19	23	37	60	48	30	71
	Deviation [cm]	2	-1	-4	-6	-1	7	3

by the mobility effects. In terms of overall fit to the empirical data (GOF), the estimated Gamma model is approximately 10x more fitted in the mobile case as compared to the static case.

In the case of the CV RTLS, the estimated Gamma distribution parameters for static human conditions present a relatively large α compared to β. This suggest that ranging errors are predominantly concentrated around the mean value, but low probability of large errors occurring. This observation may be attributed to variations in the extrinsic camera parameters, specifically in terms of height and pose. For the mobile case, the case is opposite, a relatively large β is estimated as compared to α. Also S is large in this case. This is consistent with the larger variability of the CV ranging data in the mobile case due to the inaccuracies of the CV detection and tracking algorithm. In terms of GOF, the CV RTLS models present similar levels.

The differences between the experimental data and estimated data with the Gamma models are summarized in Table 5 for various confidence levels. These results indicate that all the proposed Gamma models for predicting the position of a static or mobile human worker with either the UWB or the CV RTLSs are valid within 90% confidence level for a maximum tolerable error of 6 cm. For a 99.9% confidence level, a maximum tolerable error of 10 cm should be considered in static conditions, increased to 25-50 cm in mobile conditions. This level of accuracy suffices our needs for integrating the model into DT simulations, abstracting the parametrization and complexity of the real systems, allowing us to integrate realistic human localization behaviours in the more complex planning industrial production procedures [60].

D. DETECTION OF HUMANS NOT WEARING UWB TAGS

The individual assessment of the two RTLSs indicates that, in our operational industrial scenario, the CV system is the best for detecting a human worker in static conditions, while the UWB one performs better when the human worker is moving. However, the analysis also indicated that the performance of the UWB localization is very similar in both static and mobile conditions. Therefore, UWB should be a preferred choice of primary RTLS, and CV should be considered as a backup system. Based on this, the preferred method to guarantee safety in the industrial production scenario would be to equip human workers with tags so that they are constantly detected and tracked by the UWB system.

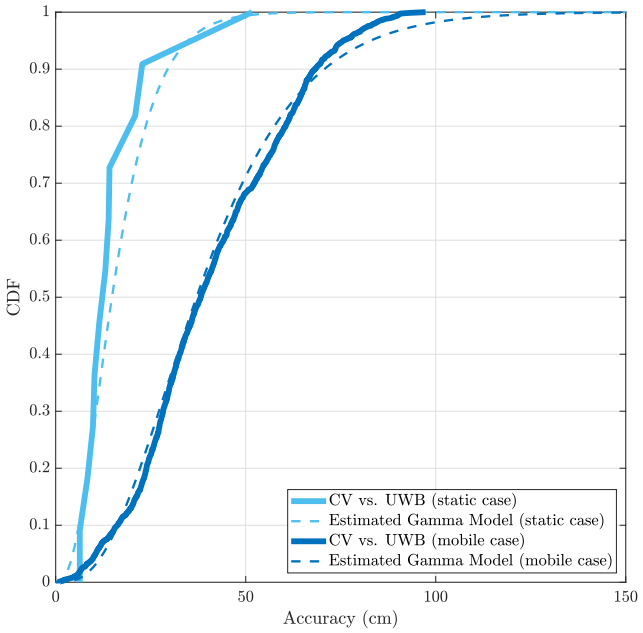

FIGURE 16. Real-time positioning difference between CV and UWB samples in static and mobile conditions.

However, in the eventual case a human worker forgets to wear the tag, or the tag fails or runs out of battery, the CV detection plays a key role.

Here, it is important to understand the potential deviations between the main source of localization (UWB) and the secondary one (CV) in order to better understand the potential safety margins that need to be considered in run-time operational safety. Fig. 16 details the CDFs of the difference between the simultaneous CV and UWB localization data (Δ) both in the static and mobile cases. The figure indicates that the real-time discrepancies between the CV and UWB readings exhibit a median value of 13 cm, increased to 52 cm as a maximum difference in static conditions; further increased to 41 cm and 97 cm in mobile settings. Such values are in good agreement with the overall UWB and CV localization performance as in the worst-case scenario, the discrepancy between the CV and UWB data in the static (mobile) case does not exceed the sum of the estimated error for the individual CV and UWB RTLSs in static (mobile) conditions. This assertion is well supported when reviewing the numerical data presented in Table 3, where the summary statistics for this case are also included. As the nature of the statistical distributions for the CV-UWB difference is right-skewed and non-symmetrical, again, the Gamma distribution is seen as a good model candidate, just as before for the individual UWB and CV localization performance. Therefore, a Gamma distribution was fitted to the empirical data and the specific parameters, fitting metrics, and comparison between model outputs are also included in Tables 4 and 5.

Understanding the bounded behavior of Δ allows us to use this metric, combined with the individual UWB and CV performance, as a safety measure for reliably detecting humans without UWB tags. Table 6 provides an overview of the potential safety radius that needs to be considered around human workers due to uncertainty in the localization in the industrial operation environment, computed as a combination of the different results provided in our assessment in the worst possible conditions. This would be applicable even in the presence of multiple humans. The two RTLSs can discriminate/distinguish between multiple targets (human workers) as each individual detected in our study is assigned a unique ID (both in the UWB and CV systems). With the known maximum distance between CV and UWB outputs for individual tracking, we can generalize our scenarios to include multiple individuals by mapping IDs from UWB to CV system. In situations where one-to-one mapping between UWB and CV is not feasible, such as when multiple individuals are close together, the current data quality would still support our objectives. As our primary goal is not to identify each individual uniquely but to ensure the detection of human presence to maintain safe distances and identify individuals without tags, we account for the worst-case scenario to ensure that our decisions are both cautious and safe. For example, on a busy manufacturing floor where workers frequently gather near machinery, the focus will be on alerting the presence of the nearest personnel within a hazard zone. Additionally, a CV and UWB data discrepancy that exceeds the maximum established distance in crowded areas can be detected, even if a one-to-one mapping between CV and UWB data cannot be established. This approach ensures robust safety measures are in place to handle dynamic and densely populated environments.

In run-time operation, simultaneous readings from the primary UWB RTLS and the secondary CV RTLS are evaluated. If UWB samples and CV samples are separated by less than 0.52 m (0.97 m) in static (mobile) situations, it can be estimated that the human worker is wearing an operational UWB tag and is also detected by the secondary CV system. In this case, nominal safety margins relate directly to the levels of uncertainty in the output of the primary UWB RTLS. However, in the potential case that there is only a CV sample, or simultaneous UWB and CV samples are separated by more than 0.52 m (0.97 m) in static (mobile) conditions; then this means that one human worker is detected by the CV system but not by the UWB system, or that one human worker is detected by the CV system and another human worker is detected by the UWB system. In this case, we have detected a hazard situation where a human worker is not equipped with an UWB tag, or is equipped with a malfunctioning UWB tag. Therefore, an alert to the human worker should be issued while the operational safety margins are adapted consequently to account for the further uncertainty in the localization.

From Table 6, it can be concluded that 1 m would be an appropriate human localization safety margin in nominal conditions, which should be doubled to 2 m in the presence of a potential hazard situation. This information would be extremely relevant in operational industrial environments in

TABLE 6. Operational safety margins to be considered in human worker localization in different industrial conditions for 50%, 90% and 99% confidence levels.

	Nominal Safety		Hazard Situation	
	Static Human Worker	Mobile Human Worker	Static Human Worker	Mobile Human Worker
99.9% [m]	0.93	0.79	1.45	1.76
90% [m]	0.41	0.47	0.93	1.44
50% [m]	0.19	0.23	0.71	1.20

the case of having a centralized control entity, such as the DT detailed in Section I, controlling and optimizing the overall factory production flows according to the inputs from RTLSs. This would allow to establish tailored virtual safety radius around human workers and identify and signal in advance, whether a human worker could constitute a potential obstacle in the route of an AMR; or seen from the other perspective, whether an AMR could be a potential hazard for a human worker.

At present, safety standards for AMRs in industrial environments do not allow the use or integration of external RTLSs in any of the safety decision-making procedures [61]. This means that, currently, an autonomous robotic entity should react to the presence of a human in the environment based only on the readings from its own onboard sensors, configured according to the adaptive protective field settings set by the regulations [62], [63]. Current protective field ranges for human detection are AMR speed-dependent, and vary between 0.08 m and 1.35 m when driving backwards at 0.1 and 1 m/s, respectively. When driving forward, the values are variable between 0.08 m and 2.85 m at 0.1 and 2.1 m/s, respectively [64]. In the most challenging case, which corresponds to AMRs operating at the highest speed, these values are at the same level of our estimated safety margins in human localization. This means that, if in the future, regulations for operational safety in presence of mobile robotic elements are updated to allow for the use of external up-to-date information from the location of other entities (including humans), simplified protective field measures could be implemented in the AMRs, enhancing global safety in the operational environment while reducing the onboard sensors computing needs and overall power consumption (thus, enlarging the autonomy of the mobile robotic entity, and increasing production throughput).

V. CONCLUSION AND FUTURE WORK

This paper evaluated and modeled the accuracy of two Real Time Location Systems (RTLSs), one based on Ultra Wideband (UWB) radio, and one based on Computer Vision (CV) in an operation industrial setup, where human workers and autonomous mobile robots (AMRs) operate in close proximity, with the primary objective of enhancing safety and efficiency in production procedures. The experimental results demonstrated that, in the considered scenario, both RTLSs can achieve comparable levels of median accuracy in the order of tenths of cm (12-19 cm) in human static conditions, which are degraded to 23-25 cm if the worker is moving. The empirical performance (accuracy) by the two RTLSs in the different operational conditions was modelled by means of Gamma distributions of the resulting error functions, with a maximum tolerable error of 5 cm at 90% confidence levels. The observed levels of accuracy are similar to those achieved by the commercial AMRs' built-in locating systems, which demonstrates that the deployed RTLSs are an effective and reliable source of human worker positioning information, useful for utilization in centralized monitoring and control entities (e.g., industrial digital twins) for overall runtime production process optimization. The experimental data also indicates that utilizing UWB as the primary source of human detection in the production environment, and CV as a backup, assuming operational safety margins of 1 m in nominal conditions and 2 m in case of hazardous situations (e.g., a human worker is not wearing the UWB tag, or the UWB tag is missing or malfunctioning) would result at levels similar to those from the protective fields ranges stated in current safety standards for AMRs in proximity of humans.

Future research will focus on extending the accuracy performance analysis by considering different industrial scenarios with different clutter topologies and RTLSs deployment configurations, and potentially developing a generalized positioning accuracy model. The use of RTLS data in industrial digital twins will be leveraged further by optimizing the operational AMR routes and overall path and mission planning based on human worker locations and behaviours (e.g., dynamic route adjustments based on up-to-date location information, offering potential for collision reduction, deadlock prevention, and minimizing slowdowns in industrial environments).

REFERENCES

[1] S. Thiede, B. Sullivan, R. Damgrave, and E. Lutters, "Real-time locating systems (RTLS) in future factories: Technology review, morphology and application potentials," *Proc. CIRP*, vol. 104, pp. 671–676, Jan. 2021.

[2] G. A. Bekey, *Autonomous Mobile Robots: Sensing, Control, Decision Making, and Applications*. Cambridge, MA, USA: MIT Press, 2005.

[3] C. Drabek, A. Kosmalska, G. Weiss, T. Ishigooka, S. Otsuka, and M. Mizuochi, "Safe interaction of automated forklifts and humans at blind corners in a warehouse with infrastructure sensors," in *Computer Safety, Reliability, and Security*, I. Habli, M. Sujan, and F. Bitsch, Eds. Cham, Switzerland: Springer, 2021, pp. 163–177.

[4] A. Löcklin, F. Dettinger, M. Artelt, N. Jazdi, and M. Weyrich, "Trajectory prediction of workers to improve AGV and AMR operation based on the manufacturing schedule," *Proc. CIRP*, vol. 107, pp. 283–288, Jan. 2022.

[5] J. Zenkert, C. Weber, M. Dornhöfer, H. Abu-Rasheed, and M. Fathi, "Knowledge integration in smart factories," *Encyclopedia*, vol. 1, no. 3, pp. 792–811, Aug. 2021.
[6] J. Stenerson, *Industrial Automation and Process Control*. Upper Saddle River, NJ, USA: Prentice-Hall, 2003.
[7] M. Wolf, M. Rantschl, E. Auberger, H. Preising, A. Sbaragli, F. Pilati, and C. Ramsauer, "Real time locating systems for human centered production planning and monitoring," *IFAC-PapersOnLine*, vol. 55, no. 2, pp. 366–371, 2022.
[8] E. M. Martinez, P. Ponce, I. Macias, and A. Molina, "Automation pyramid as constructor for a complete digital twin, case study: A didactic manufacturing system," *Sensors*, vol. 21, no. 14, p. 4656, Jul. 2021.
[9] Y. Jiang, S. Yin, K. Li, H. Luo, and O. Kaynak, "Industrial applications of digital twins," *Philos. Trans. Roy. Soc. A, Math., Phys. Eng. Sci.*, vol. 379, no. 2207, 2207, Art. no. 20200360.
[10] M. Attaran, S. Attaran, and B. G. Celik, "The impact of digital twins on the evolution of intelligent manufacturing and Industry 4.0," *Adv. Comput. Intell.*, vol. 3, no. 3, p. 11, Jun. 2023.
[11] T. Ruppert and J. Abonyi, "Integration of real-time locating systems into digital twins," *J. Ind. Inf. Integr.*, vol. 20, Dec. 2020, Art. no. 100174.
[12] M. Boldo, N. Bombieri, S. Centomo, M. De Marchi, F. Demrozi, G. Pravadelli, D. Quaglia, and C. Turetta, "Integrating wearable and camera based monitoring in the digital twin for safety assessment in the Industry 4.0 era," in *Leveraging Applications of Formal Methods, Verification and Validation. Practice*, T. Margaria and B. Steffen, Eds. Cham, Switzerland: Springer, 2022, pp. 184–194.
[13] S. J. Hayward, K. van Lopik, C. Hinde, and A. A. West, "A survey of indoor location technologies, techniques and applications in industry," *Internet Things*, vol. 20, Nov. 2022, Art. no. 100608.
[14] M. Elsanhoury, P. Mäkelä, J. Koljonen, P. Välisuo, A. Shamsuzzoha, T. Mantere, M. Elmusrati, and H. Kuusniemi, "Precision positioning for smart logistics using ultra-wideband technology-based indoor navigation: A review," *IEEE Access*, vol. 10, pp. 44413–44445, 2022.
[15] A. Schjørring, A. L. Cretu-Sircu, I. Rodriguez, P. Cederholm, G. Berardinelli, and P. Mogensen, "Performance evaluation of a UWB positioning system applied to static and mobile use cases in industrial scenarios," *Electronics*, vol. 11, no. 20, p. 3294, Oct. 2022.
[16] F. B. Islam, J. Lee, and D. Kim, "Smart factory floor safety monitoring using UWB sensor," *IET Sci., Meas. Technol.*, vol. 16, no. 7, pp. 412–425, Sep. 2022.
[17] S. Sellak, O. Haberchad, S. Ibenyahia, and Y. Salih-Alj, "Safety management system for factory workers using UWB indoor positioning and wearable vibrotactile guidance: Morocco case study," in *Proc. IEEE Int. Conf. Mechatronics Autom. (ICMA)*, Aug. 2023, pp. 1509–1514.
[18] J. Karedal, S. Wyne, P. Almers, F. Tufvesson, and A. Molisch, "A measurement-based statistical model for industrial ultra-wideband channels," *IEEE Trans. Wireless Commun.*, vol. 6, no. 8, pp. 3028–3037, Aug. 2007.
[19] T. Otim, A. Bahillo, L. E. Díez, P. Lopez-Iturri, and F. Falcone, "Impact of body wearable sensor positions on UWB ranging," *IEEE Sensors J.*, vol. 19, no. 23, pp. 11449–11457, Dec. 2019.
[20] Q. Tian, K. I. Wang, and Z. Salcic, "Human body shadowing effect on UWB-based ranging system for pedestrian tracking," *IEEE Trans. Instrum. Meas.*, vol. 68, no. 10, pp. 4028–4037, Oct. 2019.
[21] C. De Cock, E. Tanghe, W. Joseph, and D. Plets, "Robust IMU-based mitigation of human body shadowing in UWB indoor positioning," *Sensors*, vol. 23, no. 19, p. 8289, Oct. 2023.
[22] H. Zhang, Q. Wang, C. Yan, J. Xu, and B. Zhang, "Research on UWB indoor positioning algorithm under the influence of human occlusion and spatial NLOS," *Remote Sens.*, vol. 14, no. 24, p. 6338, Dec. 2022.
[23] A. R. Jiménez and F. Seco, "Comparing decawave and bespoon UWB location systems: Indoor/outdoor performance analysis," in *Proc. Int. Conf. Indoor Positioning Indoor Navigat. (IPIN)*, Oct. 2016, pp. 1–8.
[24] A. R. Jiménez and F. Seco, "Improving the accuracy of Decawave's UWB MDEK1001 location system by gaining access to multiple ranges," *Sensors*, vol. 21, no. 5, p. 1787, Mar. 2021.
[25] P. Wu, "Comparison between the ultra-wide band based indoor positioning technology and other technologies," *J. Phys., Conf. Ser.*, vol. 2187, no. 1, Feb. 2022, Art. no. 012010.
[26] D.-H. Kim and J.-Y. Pyun, "NLOS identification based UWB and PDR hybrid positioning system," *IEEE Access*, vol. 9, pp. 102917–102929, 2021.
[27] X. Yang, J. Wang, D. Song, B. Feng, and H. Ye, "A novel NLOS error compensation method based IMU for UWB indoor positioning system," *IEEE Sensors J.*, vol. 21, no. 9, pp. 11203–11212, May 2021.
[28] C. Wang, A. Xu, J. Kuang, X. Sui, Y. Hao, and X. Niu, "A high-accuracy indoor localization system and applications based on tightly coupled UWB/INS/Floor map integration," *IEEE Sensors J.*, vol. 21, no. 16, pp. 18166–18177, Aug. 2021.
[29] B. Yang, J. Li, and H. Zhang, "Resilient indoor localization system based on UWB and visual–inertial sensors for complex environments," *IEEE Trans. Instrum. Meas.*, vol. 70, pp. 1–14, 2021.
[30] P. Peng, C. Yu, Q. Xia, Z. Zheng, K. Zhao, and W. Chen, "An indoor positioning method based on UWB and visual fusion," *Sensors*, vol. 22, no. 4, p. 1394, Feb. 2022.
[31] H. Sadruddin, A. Mahmoud, and M. Atia, "An indoor navigation system using stereo vision, IMU and UWB sensor fusion," in *Proc. IEEE Sensors*, Oct. 2019, pp. 1–4.
[32] A. Morar, A. Moldoveanu, I. Mocanu, F. Moldoveanu, I. E. Radoi, V. Asavei, A. Gradinaru, and A. Butean, "A comprehensive survey of indoor localization methods based on computer vision," *Sensors*, vol. 20, no. 9, p. 2641, May 2020.
[33] R. Mosberger and H. Andreasson, "An inexpensive monocular vision system for tracking humans in industrial environments," in *Proc. IEEE Int. Conf. Robot. Autom.*, May 2013, pp. 5850–5857.
[34] S. Papaioannou, H. Wen, A. Markham, and N. Trigoni, "Fusion of radio and camera sensor data for accurate indoor positioning," in *Proc. IEEE 11th Int. Conf. Mobile Ad Hoc Sensor Syst.*, Oct. 2014, pp. 109–117.
[35] N. Zengeler, A. Arntz, D. Keßler, M. Grimm, Z. Qasem, M. Jansen, S. Eimler, and U. Handmann, "Person tracking in heavy industry environments with camera images," in *Science and Technologies for Smart Cities*, H. Santos, G. V. Pereira, M. Budde, S. F. Lopes, and P. Nikolic, Eds. Cham, Switzerland: Springer, 2020, pp. 324–336.
[36] T. Partanen, P. Mller, J. Collin, and J. Bjrklund, "Implementation and accuracy evaluation of fixed camera-based object positioning system employing CNN-detector," in *Proc. 9th Eur. Workshop Vis. Inf. Process. (EUVIP)*, 2021, pp. 1–6.
[37] L. E. O. Fernandez, "Method to measure, model, and predict depth and positioning errors of RGB-D cameras in function of distance, velocity, and vibration," Ph.D. dissertation, Federal Univ. Rio Grande do Norte, Natal, RN, USA, Jun. 2021.
[38] T. Dieterle, F. Particke, L. Patino-Studencki, and J. Thielecke, "Sensor data fusion of LiDAR with stereo RGB-D camera for object tracking," in *Proc. IEEE Sensors*, Oct. 2017, pp. 1–3.
[39] X. Ma, Y. Zhang, D. Xu, D. Zhou, S. Yi, H. Li, and W. Ouyang, "Delving into localization errors for monocular 3D object detection," in *Proc. IEEE/CVF Conf. Comput. Vis. Pattern Recognit. (CVPR)*, Jun. 2021, pp. 4719–4728.
[40] A. S. Olagoke, H. Ibrahim, and S. S. Teoh, "Literature survey on multi-camera system and its application," *IEEE Access*, vol. 8, pp. 172892–172922, 2020.
[41] T. I. Amosa, P. Sebastian, L. I. Izhar, O. Ibrahim, L. S. Ayinla, A. A. Bahashwan, A. Bala, and Y. A. Samaila, "Multi-camera multi-object tracking: A review of current trends and future advances," *Neurocomputing*, vol. 552, Oct. 2023, Art. no. 126558.
[42] Á. Utasi and C. Benedek, "A Bayesian approach on people localization in multicamera systems," *IEEE Trans. Circuits Syst. Video Technol.*, vol. 23, no. 1, pp. 105–115, Jan. 2013.
[43] L. Sun, H. Di, L. Tao, and G. Xu, "A robust approach for person localization in multi-camera environment," in *Proc. 20th Int. Conf. Pattern Recognit.*, Aug. 2010, pp. 4036–4039.
[44] J. Shen, W. Yan, P. Miller, and H. Zhou, "Human localization in a cluttered space using multiple cameras," in *Proc. 7th IEEE Int. Conf. Adv. Video Signal Based Surveill.*, Aug. 2010, pp. 85–90.
[45] I. Siriwat, T. Theeramankong, I. Methasate, and H. Kunieda, "Multi-camera based human localization for room utilization monitoring system," in *Proc. 11th Int. Joint Conf. Comput. Sci. Softw. Eng. (JCSSE)*, May 2014, pp. 46–51.
[46] *AAU 5G Smart Production Lab Web Page*. Accessed: Dec. 15, 2023. [Online]. Available: https://www.5gsmartproduction.aau.dk
[47] F. Liu, J. Zhang, J. Wang, H. Han, and D. Yang, "An UWB/Vision fusion scheme for determining Pedestrians' indoor location," *Sensors*, vol. 20, no. 4, p. 1139, Feb. 2020.

[48] R. Inam, K. Raizer, A. Hata, R. Souza, E. Forsman, E. Cao, and S. Wang, "Risk assessment for human-robot collaboration in an automated warehouse scenario," in *Proc. IEEE 23rd Int. Conf. Emerg. Technol. Factory Autom. (ETFA)*, vol. 1, Sep. 2018, pp. 743–751.
[49] *Leica TS16: Robotic Total Station*. Accessed: Dec. 15, 2023. [Online]. Available: https://leica-geosystems.com/products/total-stations/robotic-total-stations/leica-ts16
[50] *Pozyx UWB Anchors*. Accessed: Dec. 15, 2023. [Online]. Available: https://www.pozyx.io/products/hardware/hardware-anchors.
[51] *Pozyx UWB Developer Tag Specifications*. Accessed: Dec. 15, 2023. [Online]. Available: https://www.pozyx.io/products/hardware/tags/developer-tag
[52] B. Mishra and A. Kertesz, "The use of MQTT in M2M and IoT systems: A survey," *IEEE Access*, vol. 8, pp. 201071–201086, 2020.
[53] *HIKVISION DS-2TD1217-2/PA Thermal and Optical Bi-spectrum Network Turret Camera Specifications*. Accessed: Dec. 15, 2023. [Online]. Available: https://us.hikvision.com/en/products/more-products/discontinued-products/thermal-camera/thermal-and-optical-network-turret
[54] *Ambolt AI. Mobile Robots Must Learn to Drive Nicely Among People*. Accessed: Dec. 15, 2023. [Online]. Available: https://ambolt.io/en/mobile-robots-must-learn-to-drive-nicely-among-people/
[55] A. Bochkovskiy, C.-Y. Wang, and H.-Y. M. Liao, "YOLOv4: Optimal speed and accuracy of object detection," 2020, *arXiv:2004.10934*.
[56] O. Faugeras, *Three-Dimensional Computer Vision: A Geometric Viewpoint*. Cambridge, MA, USA: MIT Press, 1993.
[57] W. Haynes, *Maximum Likelihood Estimation*. New York, NY, USA: Springer, 2013, pp. 1190–1191.
[58] B. Illowsky and S. Dean, *Statistics*. Houston, TX, USA: OpenStax, Mar. 2020.
[59] C. D. Schunn et al., "Evaluating goodness-of-fit in comparison of models to data," in *Psychologie der Kognition: Reden and Vorträge Anlässlich der Emeritierung von Werner Tack*. Saarbrücken, Germany: Univ. of Saarland Press, 2005, pp. 115–154.
[60] N. Bouaziz, B. Bettayeb, M. Sahnoun, A. Yassine, and A. Latreche, "Modeling and simulation of human behavior impact on production throughput," *IFAC-PapersOnLine*, vol. 55, no. 10, pp. 1740–1745, 2022.
[61] *Safety of Industrial Trucks Driverless Trucks and Their Systems*, Standard BS EN 1525, 1998.
[62] R. Bogue, "Robots that interact with humans: A review of safety technologies and standards," *Ind. Robot: Int. J.*, vol. 44, no. 4, pp. 395–400, Jun. 2017.
[63] R. Bostelman, T. Hong, R. Madhavan, and T. Chang, "Safety standard advancement toward mobile robot use near humans," in *Proc. RIA SIAS 4th Int. Conf. Saf. Ind. Automated Syst.*, Chicago, IL, USA, 2006, pp. 1–8. [Online]. Available: https://tsapps.nist.gov/publication/getpdf.cfm?pubid=822685
[64] Mobile Industrial Robots A/S, MiR250 user guide. (2020). *Mobile Industrial Robots A/S (MiR)*. [Online]. Available: https://www.mobile-industrial-robots.com/

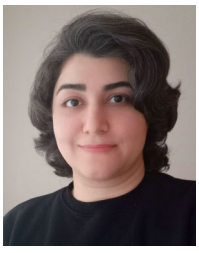

SEPIDEH VALIOLLAHI received the B.S., M.S., and Ph.D. degrees in electronics from Babol Noshirvani University of Technology, Babol, Iran, in 2009, 2012, and 2018, respectively. She is currently a Postdoctoral Researcher with Aalborg University, Aalborg, Denmark. Her current research interests include industrial digital twins, mobile robotics, artificial intelligence, machine learning, and signal processing.

IGNACIO RODRIGUEZ received the combined B.Sc. and M.Sc. degrees in telecommunication engineering from the University of Oviedo, Spain, in 2016, and the M.Sc. degree in mobile communications and the Ph.D. degree in wireless communications from Aalborg University, Denmark, in 2011 and 2016, respectively. He is currently a Ramon y Cajal Research Fellow with the University of Oviedo, Spain. Previously, he was an Assistant Professor with Aalborg University, where he led the 5G for Industries Research Group and an External Research Engineer with Nokia Bell Laboratories, where he was mainly involved in 3GPP and ITU-R standardization activities. His research interests include radio propagation, ultra-reliable and low-latency communications, and the Industrial IoT. He was a co-recipient of the IEEE VTS 2017 Neal Shepherd Memorial Best Propagation Paper Award. He was co-awarded with the 5G-prize by the Danish Energy Agency and the Danish Society of Telecommunication Engineers, in 2019.

WEIFAN ZHANG received the B.S. degree from Henan University, in 2014, and the M.S. degree from Fuzhou University, in 2018. He is currently pursuing the Ph.D. degree with Aalborg University, Aalborg, Denmark. From 2018 to 2020, he was with Huawei Technologies Company Ltd. His research interests include cloud computing and the IIoT communication.

HIMANSHU SHARMA received the B.Tech. degree in electronics and communication engineering (ECE), in 2008, the M.Tech. degree in ECE from Dr. A. P. J. Abdul Kalam Technical University (AKTU), Lucknow, Uttar Pradesh, India, in 2014, and the Ph.D. degree in wireless sensor networks (WSN) and Internet of Things (IoT) from Jamia Millia Islamia (a Central Government University), New Delhi, India, in 2019. His research interests include wireless sensor networks (WSN), the Internet of Things (IoT), and machine learning algorithms.

PREBEN MOGENSEN received the M.Sc. and Ph.D. degrees from Aalborg University, in 1988 and 1996, respectively. Since 1995, he has been a part-time associated with Nokia in various research positions and have made contributions from 2G to 5G cellular technologies. He was with Aalborg University, in 1988, where he became a Full Professor, in 2000. He is currently leading the Wireless Communication Networks Section, Department of Electronic Systems, Aalborg University. He is also a Principal Scientist with the Standardization Research Laboratory, Nokia Bell Laboratories. He has coauthored over 600 articles in various domains of wireless communication and his Google Scholar H-index is 71. His current research interests include industrial use cases for 5G, 5G evolution, and 6G. He is a Bell Laboratories Fellow.